Journal of Materials Chemistry A

ROYAL SOCIETY OF CHEMISTRY

PAPER

View Article Online
View Journal | View Issue

Cite this: J. Mater. Chem. A, 2023, 11, 7670

An electrolyte additive for the improved high voltage performance of $LiNi_{0.5}Mn_{1.5}O_4$ (LNMO) cathodes in Li-ion batteries†

Minh Tri Nguyen, [a] Hieu Quang Pham,[b] José Augusto Berrocal, [a] Ilja Gunkel *[a] and Ullrich Steiner *[a]

High-voltage cathode materials are important for the implementation of high-energy-density Li-ion batteries. However, with increasing cut-off voltages, interfacial instabilities between electrodes and the electrolyte limit their commercial development. This study addresses this issue by proposing a new electrolyte additive, (3-aminopropyl)triethoxysilane (APTS). APTS stabilises the interface between the $LiNi_{0.5}Mn_{1.5}O_4$ (LNMO) cathode and the electrolyte in LNMO||Li half-cells due to its multifunctional character. The amino groups in APTS facilitate the formation of a robust protective cathode layer. Its silane groups improve layer stability by neutralising the electrolyte's detrimental hydrogen fluoride and water. Electrochemical measurements reveal that the addition of 0.5 wt% APTS significantly improves the long-term cycling stability of LNMO||Li half-cells at room temperature and 55 °C. APTS-addition to the electrolyte delivers excellent capacity retention of 92% after 350 cycles at room temperature and 71% after 300 cycles at 55 °C (1C) contrasting with the much lower performances of the additive-free electrolyte. The addition of a 0.5 wt% (3-glycidyloxypropyl)trimethoxysilane (GLYMO) additive, which contains only the siloxane group, but lacks the amine group, displayed a capacity retention of 73% after 350 cycles at room temperature but degraded significantly upon cycling at 55 °C.

Received 21st December 2022
Accepted 14th February 2023

DOI: 10.1039/d2ta09930f

rsc.li/materials-a

Introduction

Lithium-ion batteries (LIBs) are widely applied for transportation and power applications and have been subject to ongoing modification to satisfy the requirements of increasing power and energy densities.[1–3] In recent years, the potentially cheap and environmentally friendly spinel $LiNi_{0.5}Mn_{1.5}O_4$ (LNMO) has been explored as a LIB cathode material. LIBs with LNMO cathodes have a high specific capacity of 147 mA h g^{-1} and a high energy density of 650 w h kg^{-1} stemming from its high operating voltage of 4.75 V *vs.* Li/Li^+, which are much higher compared to those of the popular cathode materials $LiCoO_2$ (518 w h kg^{-1}), $LiFePO_4$ (495 w h kg^{-1}), spinel-$LiMn_2O_4$ (400 w h kg^{-1}) and $LiCo_{1/3}Ni_{1/3}Mn_{1/3}O_2$ (576 w h kg^{-1}).[4–7]

However, the mass application of LNMO-based LIBs is seriously hindered by the electrochemical instability of the conventional carbonate electrolyte above 4.2 V.[8–10] Cycling LIBs at high voltages causes fast capacity fading[11,12] and metal ion dissolution at the LNMO electrode, particularly at elevated temperatures.[13–16]

Enhancing the electrochemical performance of the LNMO cathode is, therefore, crucial to stabilise the cathode/electrolyte interface at high voltages. Using oxidative electrolyte additives is considered a simple and effective approach to achieving this goal.[17–21] These additives are preferentially oxidised to form a protective layer on the cathode surface, suppressing the decomposition of the electrolyte and transition metal ion dissolution. Various additives enabling high-voltage cathode materials have been reported, including borates,[22,23] fluorides,[24,25] and sulfonates.[26–28] Among these, additives containing elemental silicon are highly promising.

Si-based electrolyte additives have recently received substantial attention as effective functional additives for high-voltage LNMO cathodes.[29–33] Using allyloxytrimethylsilane (AMSL) as an electrolyte additive, Chen *et al.*[29] improved the discharge capacity retention of a Li||LNMO half-cell from 73.1% to 80.2% after 500 cycles at room temperature and from 52.4% to 92.5% after 100 cycles at 55 °C. Xu *et al.*[30] demonstrated that the addition of tris(trimethylsilyl) phosphite (TMSP) and 1,3-propanediolcyclic sulfate (PCS) improved LNMO||MCMB (mesocarbon microbeads) full-cells at both room temperature and 50 °C, where TMSP stabilises the $LiPF_6$ salt and scavenges corrosive HF in the electrolyte. Lee *et al.*[31] proposed 4-(trimethylsiloxy)-3-pentene-2-one (TMSPO) as an electrolyte additive to enhance the cycle retention and coulombic efficiency of both Li||LNMO half-cells and graphite||LNMO full-cells. Li *et al.*[32]

[a]Adolphe Merkle Institute, University of Fribourg, Chemin des Verdiers 4, 1700 Fribourg, Switzerland. E-mail: ilja.gunkel@unifr.ch; ullrich.steiner@unifr.ch

[b]Morrow Batteries, Havnegaten 2, 4836 Arendal, Norway

† Electronic supplementary information (ESI) available. See DOI: https://doi.org/10.1039/d2ta09930f

reported that pentafluorophenyltriethoxysilane (TPS) containing elemental Si and F not only forms a stable protective cathode electrolyte interphase but also scavenges detrimental HF, resulting in increased capacity retention of up to 85% from 28% after 400 cycles at room temperature, with a C-rate of 1. Very recently, Dong *et al.*[33] demonstrated that the multifunctional electrolyte additive 1,3-divinyltetramethyldisiloxane (DTMDS) enhances the performance of Li||LNMO half-cells at room temperature.

A multifunctional additive is desirable to improve long-term cycling stability at elevated temperatures. To this end, amino-based and silane compounds with Si–O bonds have been selected. The former are favourable for forming a robust protective layer on the cathode surface.[34,35] The latter capture detrimental HF and H_2O in the electrolyte and create an ionically conductive cathode-electrolyte-interphase (CEI) layer on the cathode surface, preventing metal dissolution from the cathode.[36–40]

In this work, we propose a novel multifunctional electrolyte additive, (3-aminopropyl)triethoxysilane (APTS), to improve the cycle stability of the LNMO electrode at room temperature and 55 °C. We study the effect of APTS, which contains siloxane and amino functional groups, on interfacial stabilisation and the long-term cycling performance of Li||LNMO half-cells compared to (3-glycidyloxypropyl)trimethoxysilane (GLYMO), which only contains a siloxane group.

Materials and methods

Electrode and electrolyte preparation

The cathode material was made of 80 wt% commercial $LiNi_{0.5}Mn_{1.5}O_4$ (LNMO, MTI Corporation, USA), 10 wt% conductive carbon black (Super C65, Imerys Graphite, Switzerland, Ltd.), and 10 wt% polyvinylidene fluoride (PVDF, Kynar, ARKEMA Innovative Chemistry, USA) with *N*-methyl-2-pyrrolidone (NMP, Sigma-Aldrich, Germany) used as the solvent. The mixed powders were shaken for 30 minutes to enable the formation of a homogeneous slurry. The slurry was cast onto pieces of Al-foil and dried at 80 °C for 6 h in a vacuum oven. The dried electrode was punched into 7/16 inch diameter discs and vacuum-dried at 120 °C in a vacuum oven overnight to remove the absorbed water and remaining NMP solvent. The electrodes were then introduced into an argon-filled glovebox for assembly into coin cells. The often used electrolyte 1 M lithium hexafluorophosphate ($LiPF_6$) in 1 : 1 : 1 (v/v/v) ethylene carbonate (EC): dimethyl carbonate (DMC): diethyl carbonate (DEC) (Sigma-Aldrich, Germany) without and with 0.5, 1.5, and 5.0 wt% (3-aminopropyl)triethoxysilane (APTS, Sigma-Aldrich, Germany) or (3-glycidyloxypropyl)trimethoxysilane (GLYMO, Sigma-Aldrich, Germany) was prepared in an argon-filled glovebox. The chemical structures of solvents and additives are shown in Fig. S3.†

Density functional theory calculations

Density functional theory (DFT) calculations of the highest occupied molecular orbital (HOMO) and lowest unoccupied molecular orbital (LUMO) were obtained using the Gaussian 16 software package with the B3LYP/6-31+G(d,p) basis set.[29]

Electrochemical performance

Coin half-cells (CR2032, MTI, USA) consisting of LNMO as a working electrode, a lithium metal chip (Gelon, LIB Group, China) as a counter electrode, a separator (Grade GF/B Glass, Healthcare Life Sciences) and 300 μL electrolyte without and with different additives were assembled in an argon-filled glovebox, in which the oxygen and water contents were less than 1 ppm. Cyclic voltammetry (CV) and electrochemical impedance spectroscopy (EIS) measurements were performed with a Bio-Logic VMP 300 test system. The CV was recorded in a voltage range of 3.5 to 5.0 V *vs.* Li^+/Li, at a scan rate of 0.05 mV s^{-1}. EIS spectra were recorded in a frequency range of 200 kHz to 100 MHz with an amplitude of 5 mV. Galvanostatic charge–discharge measurements were measured using an Arbin LBT 20084 multiple channel test system in a voltage range of 3.5 to 5.0 V *vs.* Li^+/Li at room temperature and in a range of 3.5 to 4.9 V *vs.* Li^+/Li at 55 °C at a C-rate of 1 (147 mA g^{-1}) after three formation cycles at a lower C-rate of 0.1 (14.7 mA g^{-1}).

Electrode characterisation

After electrochemical cycling, the cells were disassembled in an argon-filled glovebox. The post-cycled LNMO electrodes and lithium metal disks were washed several times in DMC to remove residual electrolyte salts. The washed LNMO electrodes were then dried in the glovebox at room temperature. The surface morphologies of the LNMO electrodes caused by cycling were imaged using a scanning electron microscope (FIB-SEM, Thermo Fisher, Scios2). The uniformity and thickness of the surface layer on the LNMO electrodes that were cycled in the electrolyte without and with additives were examined using transmission electron microscopy (TEM, FEI Tecnai Spirit) at 120 kV.

Results and discussion

Oxidation and reduction behaviours of the APTS and GLYMO additives

The calculation of molecular orbital energies is helpful to predict the oxidation and reduction tendencies of organic molecules.[29,41–43] Therefore, density functional theory (DFT) calculations of the highest occupied molecular orbital (HOMO) and lowest unoccupied molecular orbital (LUMO) were performed to predict the oxidation and reduction behaviour of EC, DEC, DMC, GLYMO, and APTS, as shown in Fig. 1. According to these DFT results, the HOMO energy level of APTS is higher than those of GLYMO, EC, DEC, and DMC, indicating that APTS is preferentially oxidised on the cathode compared to GLYMO and any of the solvents of the electrolyte. These calculations agree with the CV results shown in the inset of Fig. 2.

The electrochemical behaviour of the LNMO cathode in electrolytes without and with additives was evaluated using cyclic voltammetry, as shown in Fig. 2. There are two major redox peaks at around 4.0 V and 4.75 V. The redox peak at 4.0 V

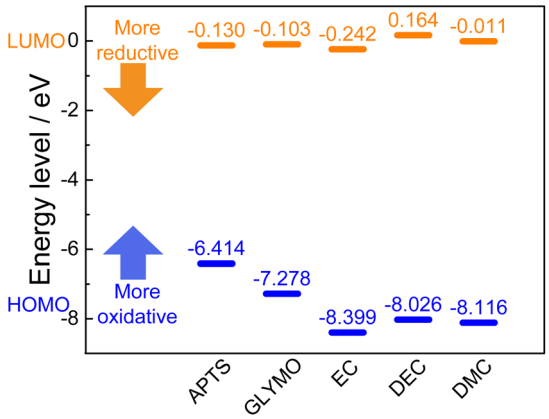

Fig. 1 Calculated LUMO and HOMO energy levels of APTS, GLYMO, EC, DEC, and DMC.

corresponds to the Mn^{3+}/Mn^{4+} couple, while the redox peak at around 4.75 V is split into two components, which correspond to the Ni^{2+}/Ni^{3+} and Ni^{3+}/Ni^{4+} couples, respectively.[44,45] Addition of APTS and GLYMO to the electrolyte gives rise to additional oxidation peaks at 4.24 V and 4.31 V, which are indicative of the oxidation of APTS and GLYMO, respectively (magnified view in Fig. 2a). These oxidation peaks disappear after 300 cycles (magnified view in Fig. 2b), suggesting that APTS and GLYMO have each completely oxidised, forming a deposit on the LNMO electrode. The pair of oxidation and reduction peaks at around 4.0 V indicates the electrochemical (de)intercalation reactions of Li^+-ions proceed in two steps, as shown in the magnified views in Fig. 2a and b.[46,47]

The potential difference between the two redox peaks (ΔE) corresponds to the degree of electrochemical polarisation (Table S1†). After the formation cycles, the electrochemical polarisation of the LNMO electrode cycled in the electrolyte without additives is slightly smaller than the electrode cycled in the electrolytes with additives. This may be related to the layer formed on the LNMO particle surface (cycled with additives), reducing the reversibility of the LNMO cathode during Li^+-(de) intercalation. However, after 300 cycles at 55 °C, the electrochemical polarisation of the LNMO electrode cycled in the electrolyte with the APTS additive is slightly increased, which may be attributed to the formation of a stable layer on the LNMO particle surface. The electrochemical polarization of the LNMO electrode increases significantly upon cycling using the neat electrolyte and the electrolyte with the GLYMO additive, suggesting that the corresponding layers formed on the electrode surface are less stable at high temperatures than the APTS-containing electrolyte.

Electrochemical cycling of Li||LNMO half-cells

The evolution of the charge and discharge profiles of Li||LNMO half-cells was investigated using the neat electrolyte and the electrolyte with either the GLYMO or APTS additive at 55 °C, as shown in Fig. 3. During cycling, the difference between the

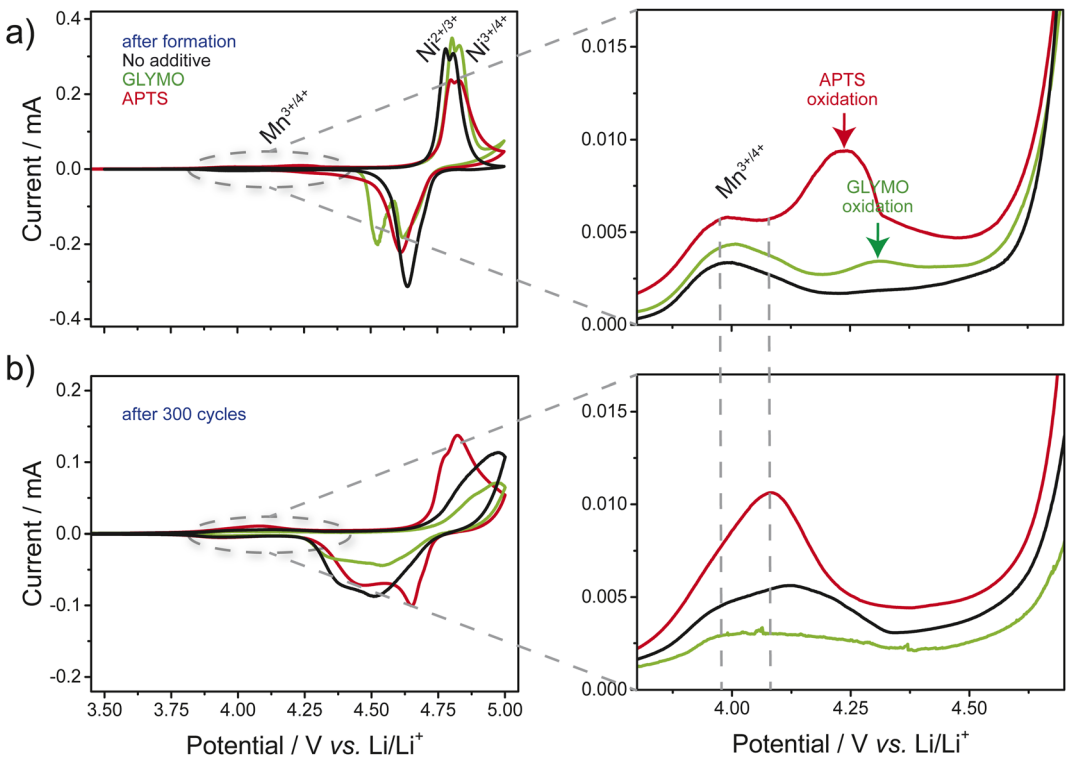

Fig. 2 CV of Li||LNMO half-cells, (a) after formation cycles and (b) after 300 cycles at 55 °C. The black, green, and red curves correspond to cells cycled using electrolytes without additives and with GLYMO and APTS additives, respectively, each measured at a scan rate of 0.05 mV s^{-1}. The insets show the magnified 3.8 V to 4.7 V region.

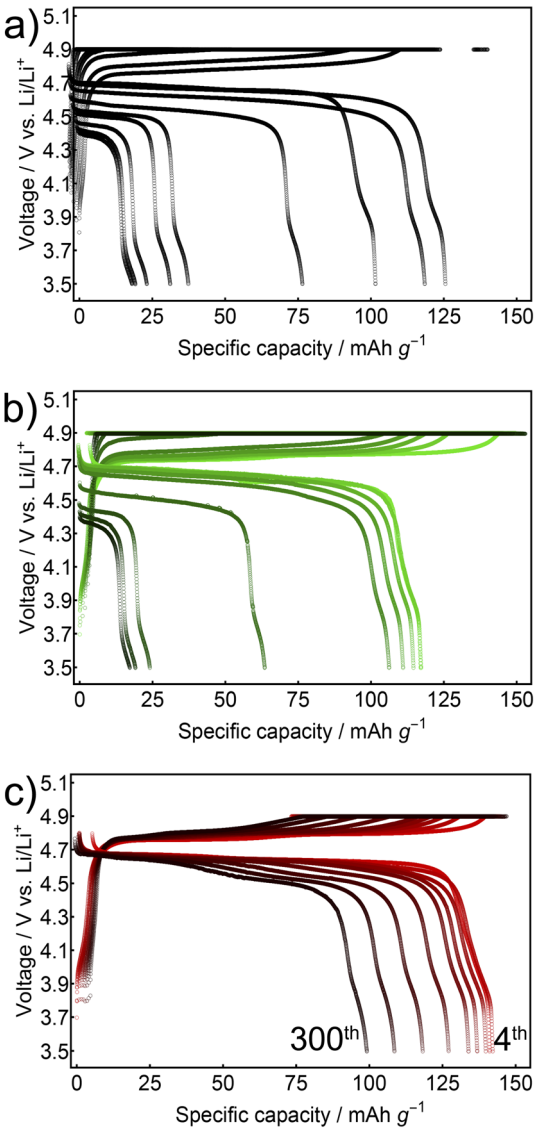

Fig. 3 Charge and discharge profiles of Li||LNMO half-cells, cycled at a C-rate of 1 between 3.5 V and 4.9 V at 55 °C in an electrolyte (a) without additives, (b) with the GLYMO additive, and (c) with the APTS additive. For each panel, nine profiles between the 4th and 300th cycles are shown.

charge and discharge plateaus gradually widens. It dramatically increases after 50 cycles in the cells containing the electrolyte without any additives (Fig. 3a). This may be related to an unstable interface between the LNMO cathode and the electrolyte. In contrast, the different charge–discharge plateaus of the GLYMO-containing electrolyte are relatively stable up to 120 cycles (Fig. 3b). Interestingly, adding APTS to the electrolyte significantly reduces the polarisation increase observed for the other two electrolytes. This cell delivers a specific discharge capacity of more than 100 mA h g^{-1} even after 300 cycles at 55 °C (Fig. 3c). This significantly improved long-term cycling stability at high temperatures is attributed to the electrode/electrolyte interface stabilisation by the APTS or GLYMO additive. The APTS additive, which contains an additional amino group compared to GLYMO, strongly enhances the cycling stability under these operating conditions.

The Li||LNMO half-cells were tested with the neat electrolyte, with the electrolyte containing optimal amounts of the 0.5 wt% GLYMO and 0.5 wt% APTS additives, respectively (Fig. S1†). Their cycling performance at a C-rate of 1 at room temperature and 55 °C is shown in Fig. 4. Adding GLYMO and APTS substantially improved the long-term cycling performance at room temperature and 55 °C. The discharge capacity retention of the LNMO cell with the neat electrolyte was reduced to only 60% after 350 cycles at room temperature. The addition of GLYMO and APTS improved the discharge capacity retention values after 350 cycles to 73% and 92%, respectively. This trend is even more pronounced at a temperature of 55 °C: the discharge capacity retention of LNMO half-cells was only 30% (after 100 cycles) and 15% (after 300 cycles) for the neat electrolyte, 91% (100 cycles) and 15% (300 cycles) for the GLYMO-containing electrolyte, and 94% (100 cycles) and 72% (300 cycles) for the APTS-containing electrolyte. The APTS additive has the most beneficial effect on long-term cycling at room- and high temperatures compared to the GLYMO additive or the absence of additives. This may be an indication that the additional amino group in APTS facilitates the formation of a protective and stable layer on the LNMO particles, in good agreement with previous reports on other cathode materials.[34,35]

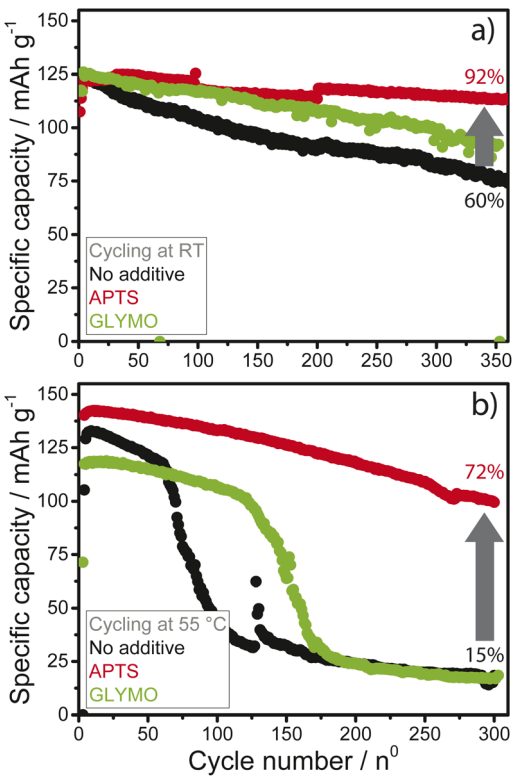

Fig. 4 Specific capacity of Li||LNMO half-cells during cycling (1C) at room temperature (a) and 55 °C (b) using the neat electrolyte (no additive), the electrolyte with APTS, and the electrolyte with the GLYMO additive.

Table 1 The effect of additives on the cycling performance of LNMO cathode materials in the present work* and previous reports[a]

			Capacity retention at RT				Capacity retention at elevated temp					
Additive (wt.)	$LiPF_6$	Electrolyte (vol.-ratio)	EL only	Additive	Cycles	C-rate	EL only	Additive	Cycles	C-rate	T °C	Cell-type	Ref.
0.5% AMSL)	1.0 M	EC/EMC/DEC (3 : 5:2)	73.1%	80.2%	500	0.5	52.4%	92.5%	100	0.5	55	Li‖LNMO	29
1.0% TMSP + 1.0% PCS	1.0 M	EC/EMC/DEC (1 : 1:1)	10.8%	79.5%	500	0.5	Failed	79.5%	200	1	50	MCMB‖ LNMO	30
0.2% TMSPO	1.3 M	EC/EMC/DEC (3 : 2:5)	Slightly improved		200	0.5	22.2%	75.5%	100	0.5	60	Li‖LNMO	31
1.0% TPS	1.0 M	EC/EMC/DEC (3 : 5:2)	28%	85%	400	1	n.a.					Li‖LNMO	32
1.0% DTMDS	1.0 M	EC/EMC (3 : 7, by wt.)	22.5%	95.32%	500	0.5	n.a.					Li‖LNMO	33
0.5% GLYMO	1.0 M	EC/DMC/DEC (1 : 1:1)	60%	73%	350	1	30%	91%	100	1	55	Li‖LNMO	*
							15%	15%	300				
0.5% APTS	1.0 M	EC/DMC/DEC (1 : 1:1)	60%	92%	350	1	30%	94%	100	1	55	Li‖LNMO	*
							15%	71%	300				

[a] EMC: ethyl methyl carbonate.

The excellent performance of the APTS-containing electrolyte is comparable to previous Si-based electrolyte additives for LNMO cathode systems. The room temperature performance of the APTS-containing electrolyte is similar to that of the DTMDS additive reported by Dong *et al.*,[33] which was, however, measured at a lower C-rate. At higher temperatures, the additive mixture of TMSP and PCS[30] gave similar results to APTS, albeit at a somewhat lower temperature and for fewer cycles. Overall, the APTS-containing electrolyte outperforms all other additives shown in Table 1.

Electrochemical impedance spectroscopy (EIS) was employed to investigate the ohmic effects of the GLYMO and APTS functional additives on the electrochemical reactions occurring at the LNMO electrode interface. EIS measurements were performed for each cell after the assembly, formation cycles, and cycling test at 55 °C. The EIS spectra of all cells consist of a depressed semicircle in the high-frequency region and a linear tail in the low-frequency region (Fig. 5). The apparent impedance differences after cycling at 55 °C are attributed to the electrolyte additives. Note that all samples show increased total impedances after cycling as shown in Fig. 5, suggesting alterations of the electrode surfaces.

The total resistance values of all LNMO cells were calculated using the equivalent circuit in the inset of Fig. 5a and are summarised in Table 2. The resistance R_1 arising from the test apparatus, including the electrolyte, connections and current collectors, was approximately 6 Ω in all measurements. R_1 remained nearly unchanged after the formation cycles. R_2 and R_3 constitute two distinct R–Q elements, which we assign to the surface film resistance and the charge transfer resistance between the electrode and electrolyte, respectively. Q_4 denotes the low-frequency Li-ion diffusion in the bulk of the electrode samples.[48]

After assembly, the total resistances of GLYMO- and APTS-containing cells were $\Sigma R_a = R_2 + R_3$ is 142.6 Ω and 178.5 Ω, respectively, which are both below the value of 207.3 Ω when no additive was added to the electrolyte. The lower resistance values in the presence of additives may indicate that the GLYMO/APTS additives accumulate on the LNMO surface, causing a decrease in resistance (Fig. 5a).[29] After the formation cycles, the total resistance of cells containing the neat and APTS-containing electrolytes increased to approximately 340 Ω, much below the 597.5 Ω of that cycled in electrolyte with the GLYMO additive (Fig. 5b). After 300 cycles at 55 °C, only the resistance of the APTS-containing cells remained close to the initial values. In contrast, the resistances of the other two cell types increased by one order of magnitude compared to the initial values (Fig. 5c). This indicates the formation of Li-ion restive layers at the cathode electrolyte interface (CEI) for the neat and GLYMO-containing electrolytes, which were absent when APTS was chosen as an electrolyte additive. The ATPS additive stabilises the CEI under these operating conditions, in contrast to the other two electrolytes.

Transmission electron microscopy (TEM) was employed to investigate CEI layer differences in the three half-cell types after 350 cycles at room temperature and after 300 cycles at 55 °C (Fig. 6). The surfaces of the pristine LNMO particles before cell

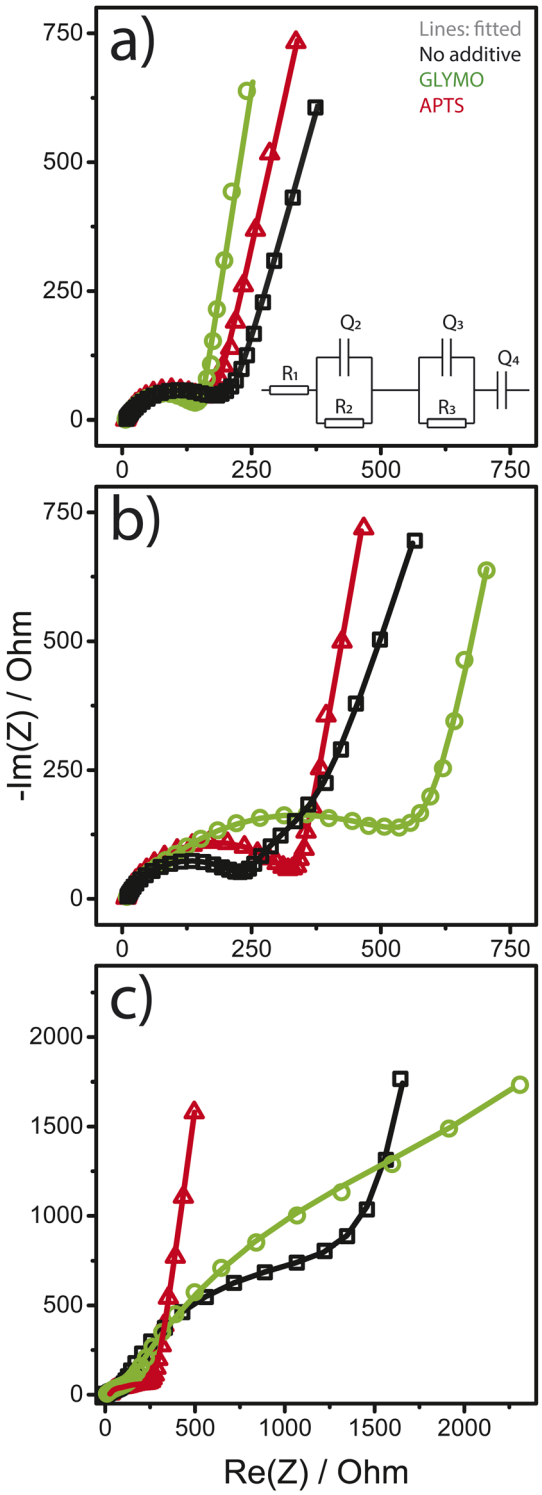

Fig. 5 Nyquist plots of Li||LNMO half-cells, (a) post-assembly, (b) after formation cycles, and (c) after 300 cycles at 55 °C. The half-cells contained electrolytes without an additive (black), with the GLYMO additive (green), and with the APTS additive (red). Shaped curves: raw EIS spectra and solid curves: fitted results. The equivalent circuit model used to fit the data is shown in the inset of (a), with the apparatus resistance R_1 and two R–Q elements corresponding to the electrolyte/LNMO and electrolyte/Li–metal interfaces, respectively. Q_4 represents Li-ion diffusion at low frequencies.

Table 2 Total resistance determined from EIS measurements of LNMO electrodes cycled in the electrolyte without any additive, the electrolyte with GLYMO, and the electrolyte with the APTS additive, (*a*) post-assembly, (*b*) after formation cycles, and (*c*) after 300 cycles at 55 °C

	Total resistance/Ω		
Sample	*a*	*b*	*c*
No additive	207.3	340.3	1548.1
GLYMO	142.6	597.5	1341.8
APTS	178.5	335.1	276

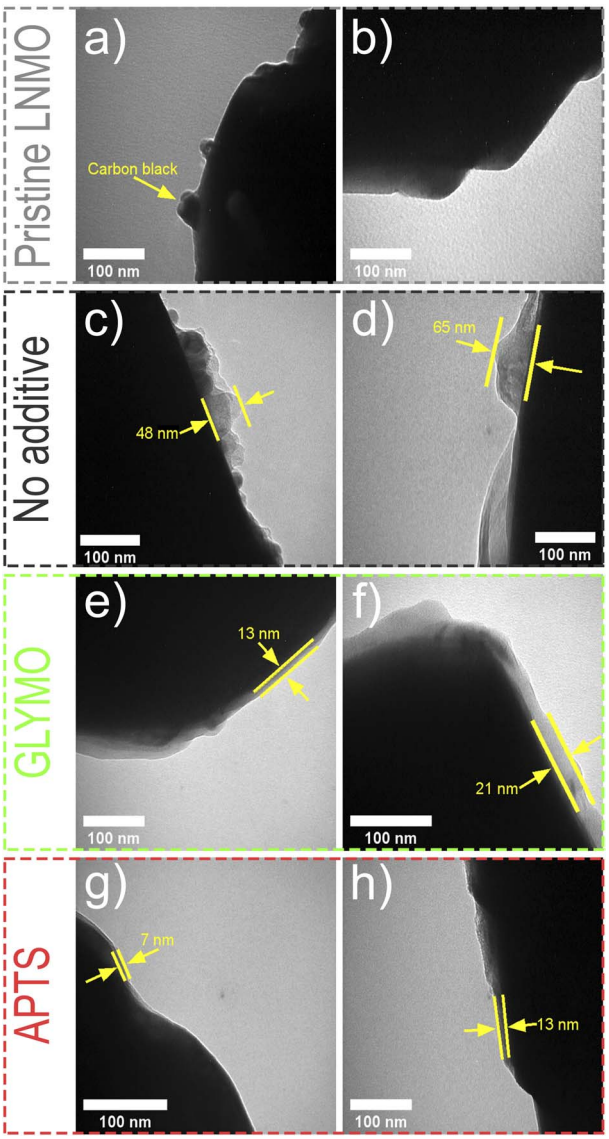

Fig. 6 TEM images of the LNMO electrodes, immediately after manufacture (a and b), after cycling in the neat electrolyte (c and d), and after cycling in the electrolyte with GLYMO (e and f), and with APTS additives (g and h). (c, e and g): After 350 cycles at RT and (d, f and h): after 300 cycles at 55 °C.

assembly are shown in Fig. 6a and b. The surface protrusions in the images are attributed to the carbon black used in the electrode manufacture. LNMO particles extracted from neat-

electrolyte cells were covered with very non-uniform CEI layers with maximal thicknesses of 48 nm and 65 nm, after 350 cycles at room temperature and 300 cycles at 55 °C as shown in Fig. 6c and d, respectively. These layers are typically composed of organic and inorganic compounds generated by the oxidation of the electrolyte,[49] which deteriorates battery performance.[50]

In contrast, when GLYMO and APTS were used as electrolyte additives, very homogeneous 7 nm to 21 nm thick CEI layers formed on the surface of the LNMO particles (Fig. 6e–h). These layers were somewhat thicker after 300 cycles at 55 °C compared to 350 cycles at room temperature. The layer thickness formed when using the APTS-containing electrolyte was approximately 1/2 that when GLYMO was employed for both cycling temperatures.

These results suggest that both additives are very effective in controlling CEI formation. While thinner, they are very homogeneous and possibly more compact, reinforcing the protection of the LNMO electrode against dissolution.

The morphology of CEI layers was further investigated by scanning electron microscopy (SEM) (Fig. 7). The surfaces of the pristine particles appear smooth and featureless (Fig. 7a and b). After cycling half-cells containing the neat electrolyte, some of the LNMO particles appear to have fractured into smaller pieces (yellow arrows), evidenced by uneven particle surfaces that differ from the crystal facets seen in the pristine particles (Fig. 7c and d). Since a CEI layer has formed during cycling, this layer probably cracked, exposing LNMO and eventually causing the particle to fracture, likely caused by the dissolution of the transition metal ions. In addition, after cycling at high temperatures, a rough layer covered the particle surfaces (Fig. S4b†), stemming from deposits caused by the decomposition of the electrolyte.

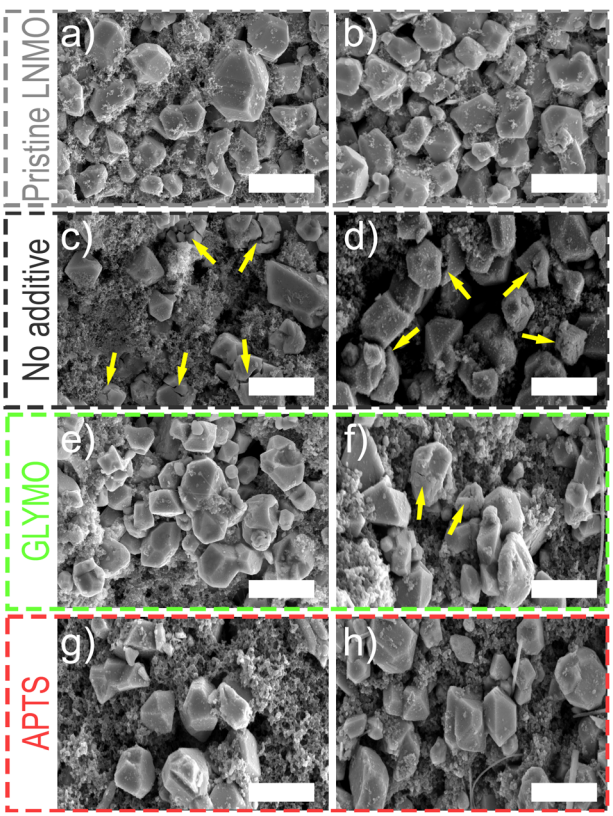

Fig. 7 SEM images of LNMO electrodes, immediately after manufacture (a and b), after cycling in the neat electrolyte (c and d), and after cycling in the electrolytes with GLYMO (e and f) and APTS (g and h) additives. (c, e and g): After 350 cycles at RT and (d, f and h): after 300 cycles at 55 °C. Scale bars: 5 μm.

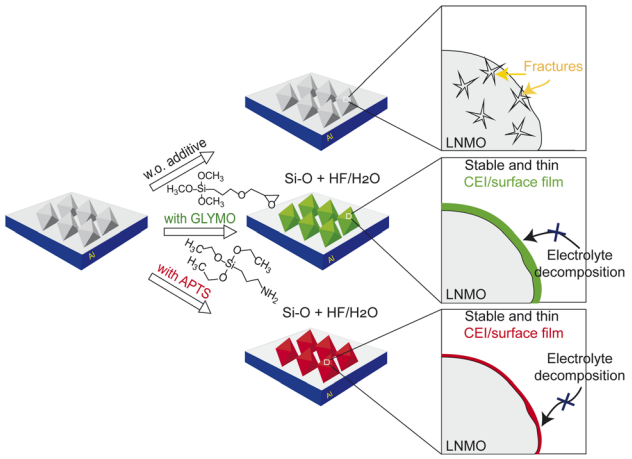

Fig. 8 Schematic illustration of CEI layer formation on LNMO cycled using (a) a neat electrolyte, (b) a GLYMO-containing electrolyte, and (c) an APTS-containing electrolyte.

In contrast, the LNMO particles extracted from half-cells cycled in GLYMO- and APTS-containing electrolytes remained highly homogeneous, even when cycled at high temperature (Fig. 7e–h). However, the LNMO grains of the GLYMO-containing cell that was cycled at 55 °C (Fig. 7f) show the appearance of some fractured particles (yellow arrows), which are absent when APTS was used as an additive (Fig. 5h).

The observations in Fig. 6 and 7 allow correlating the impedance data with the CEI layer morphology. The formation of thin, compact, and homogeneous CEI layers is essential for good cycling performance since they protect the LNMO surface from degradation while minimising the interfacial resistance.

Fig. 8 summarises our conclusions from the impedance and electron microscopy data. The preferential oxidation of GLYMO and APTS results in a comparably thin and stable CEI layer that homogeneously covers the LNMO particles. The Si–O groups in GLYMO and APTS effectively scavenge the acidic species resulting from the decomposition of the electrolyte upon cycling, thereby decreasing their detrimental effect on the LNMO particles. The additional NH_2 groups in APTS enable the formation of a homogeneous CEI film, resulting in even thinner and more robust LNMO surface layers than the layers formed for the GLYMO additive.

Conclusions

By screening through density functional theory (DFT) calculations, we identified two promising electrolyte additives, GLYMO and APTS, for the stabilisation of the interface between LNMO

electrodes and carbonate-based electrolytes. In electrochemical testing, both additives showed improved cycling performance at room temperature and 55 °C. CV measurements confirmed the DFT calculations. TEM and SEM analyses showed that APTS forms a stable and thin surface protective layer on the LNMO particles, which stayed homogeneous and intact up to 300 cycles at 55 °C.

The incorporation of 0.5 wt% GLYMO and 0.5 wt% APTS into the electrolyte of Li‖LNMO half-cells showed an excellent discharge capacity retention of 73% and 92%, respectively, after 350 cycles at room temperature, at a C-rate of 1, compared to a 60% capacity retention when no additive was added to the electrolyte. At 55 °C, a substantial improvement in cycling performance with the APTS additive was achieved, increasing the discharge capacity retention to 71% from 15% seen in both GLYMO additive and additive-free electrolyte after 300 cycles at a C-rate of 1. These results confirm APTS as a promising additive in high-voltage Li-ion batteries employing LNMO cathodes and carbonate electrolytes.

Author contributions

M. T. N. carried out the experiments. H. Q. P. contributed to the electrochemistry analysis, and J. A. B. elucidated the chemical reactions taking place at the electrodes. M. T. N designed the experimental study. M. T. N, I. G., and U. S. wrote and edited the manuscript. I. G. and U. S. supervised the project.

Conflicts of interest

There are no conflicts to declare.

Acknowledgements

The authors gratefully acknowledge the financial support from the Swiss National Science Foundation (SNSF) through the NRP70 program, grant number 153764. This study was supported by the Adolphe Merkle Foundation.

References

1 B. Horstmann, J. Shi, R. Amine, M. Werres, X. He, H. Jia, F. Hausen, I. Cekic-Laskovic, S. Wiemers-Meyer, J. Lopez, D. Galvez-Aranda, F. Baakes, D. Bresser, C.-C. Su, Y. Xu, W. Xu, P. Jakes, R.-A. Eichel, E. Figgemeier, U. Krewer, J. M. Seminario, P. B. Balbuena, C. Wang, S. Passerini, Y. Shao-Horn, M. Winter, K. Amine, R. Kostecki and A. Latz, *Energy Environ. Sci.*, 2021, **14**, 5289–5314.
2 M. Armand and J.-M. Tarascon, *Nature*, 2008, **451**, 652–657.
3 J.-M. Tarascon and M. Armand, *Nature*, 2001, **414**, 359–367.
4 T.-F. Yi, J. Mei and Y.-R. Zhu, *J. Power Sources*, 2016, **316**, 85–105.
5 R. Schmuch, R. Wagner, G. Hörpel, T. Placke and M. Winter, *Nat. Energy*, 2018, **3**, 267–278.
6 H. Xu, H. Zhang, J. Ma, G. Xu, T. Dong, J. Chen and G. Cui, *ACS Energy Lett.*, 2019, (4), 2871–2886.
7 G. Liang, V. K. Peterson, K. W. See, Z. Guo and W. K. Pang, *J. Mater. Chem. A*, 2020, **8**, 15373–15398.
8 X. Xu, S. Deng, H. Wang, J. Liu and H. Yan, *Nano-Micro Lett.*, 2017, **9**, 22.
9 Z. Zou, H. Xu, H. Zhang, Y. Tang and G. Cui, *ACS Appl. Mater. Interfaces*, 2020, (12), 21368–21385.
10 H. Wang, S. Chen, Y. Li, Y. Liu, Q. Jing, X. Liu, Z. Liu and X. Zhang, *Adv. Energy Mater.*, 2021, **11**, 2101057.
11 W. Lee, S. Muhammad, C. Sergey, H. Lee, J. Yoon, Y.-M. Kang and W.-S. Yoon, *Angew. Chem., Int. Ed.*, 2020, **59**, 2578–2605.
12 X. Yu, W. A. Yu and A. Manthiram, *Small Methods*, 2021, **5**, 2001196.
13 N. P. W. Pieczonka, Z. Liu, P. Lu, K. L. Olson, J. Moote, B. R. Powell and J.-H. Kim, *J. Phys. Chem. C*, 2013, **117**, 15947–15957.
14 J.-H. Kim, N. P. W. Pieczonka and L. Yang, *ChemPhysChem*, 2014, **15**, 1940–1954.
15 J. Ma, P. Hu, G. Cui and L. Chen, *Chem. Mater.*, 2016, **28**, 3578–3606.
16 Q. Xie, J. Chen, L. Xing, X. Zhou, Z. Ma, B. Wu, Y. Lin, H. Zhou and W. Li, *J. Energy Chem.*, 2022, **69**, 389–396.
17 H. Zhang, G. G. Eshetu, X. Judez, C. Li, L. M. Rodriguez-Martínez and M. Armand, *Angew. Chem., Int. Ed.*, 2018, **57**, 15002–15027.
18 H. Zhao, X. Yu, J. Li, B. Li, H. Shao, L. Li and Y. Deng, *J. Mater. Chem. A*, 2019, **7**, 8700–8722.
19 T. van Ree, *Curr. Opin. Electrochem.*, 2020, **21**, 22–30.
20 C. Tan, J. Yang, Q. Pan, Y. Li, Y. Li, L. Cui, X. Fan, F. Zheng, H. Wang and Q. Li, *Chem. Eng. J.*, 2021, **410**, 128422.
21 J. Chen, Z. Huang, W. Zeng, F. Cao, J. Ma, W. Tian and S. Mu, *ChemElectroChem*, 2021, **8**, 608–624.
22 T. Huang, X. Zheng, Y. Pan, Q. Li and M. Wu, *ACS Appl. Mater. Interfaces*, 2019, (11), 26872–26879.
23 Y.-Q. Chen, T.-Y. Chen, W.-D. Hsu, T.-Y. Pan, L.-J. Her, W.-M. Chang, M. Wohlfahrt-Mehrens, H. Yoshitake and C.-C. Chang, *J. Power Sources*, 2020, **477**, 228473.
24 Y. Xu, J. Liu, L. Zhou, L. Zeng and Z. Yang, *J. Electroanal. Chem.*, 2017, **791**, 109–116.
25 L. Xia, H. Miao, C. Zhang, G. Z. Chen and J. Yuan, *Energy Storage Mater.*, 2021, **38**, 542–570.
26 H. Rong, M. Xu, B. Xie, H. Lin, Y. Zhu, X. Zheng, W. Huang, Y. Liao, L. Xing and W. Li, *J. Power Sources*, 2016, **329**, 586–593.
27 G. Xu, S. Huang, Z. Cui, X. Du, X. Wang, D. Lu, X. Shangguan, J. Ma, P. Han, X. Zhou and G. Cui, *J. Power Sources*, 2019, **416**, 29–36.
28 B. Tong, Z. Song, H. Wan, W. Feng, M. Armand, J. Liu, H. Zhang and Z. Zhou, *InfoMat*, 2021, **3**, 1364–1392.
29 J. Chen, H. Zhang, M. Wang, J. Liu, C. Li and P. Zhang, *J. Power Sources*, 2016, **303**, 41–48.
30 G. Xu, C. Pang, B. Chen, J. Ma, X. Wang, J. Chai, Q. Wang, W. An, X. Zhou, G. Cui and L. Chen, *Adv. Energy Mater.*, 2018, **8**, 1701398.
31 T. J. Lee, J. Soon, S. Chae, J. H. Ryu and S. M. Oh, *ACS Appl. Mater. Interfaces*, 2019, **11**, 11306–11316.
32 H. Li, P. Zhou, F. Liu, H. Li, F. Cheng and J. Chen, *Chem. Sci.*, 2019, **10**, 1374–1379.

33 Z. Dong, J. Wei, H. Yue, K. Zhang, L. Wang, X. Li, Z. Zhang, W. Yang and S. Yang, *J. Colloid Interface Sci.*, 2021, **595**, 35–42.
34 X. Yan, C. Chen, X. Zhu, L. Pan, X. Zhao and L. Zhang, *J. Power Sources*, 2020-06-15, **461**, 228099.
35 H. Q. Pham, M. T. Nguyen, M. Tarik, M. El Kazzi and S. Trabesinger, *ChemSusChem*, 2021, **14**, 2461–2474.
36 B. Deng, H. Wang, W. Ge, X. Li, X. Yan, T. Chen, M. Qu and G. Peng, *Electrochim. Acta*, 2017, **236**, 61–71.
37 C. Wang, H. Zhang, S. Dong, Z. Hu, R. Hu, Z. Guo, T. Wang, G. Cui and L. Chen, *Chem. Mater.*, 2020, **32**, 9167–9175.
38 P. Mu, H. Zhang, H. Jiang, T. Dong, S. Zhang, C. Wang, J. Li, Y. Ma, S. Dong and G. Cui, *J. Am. Chem. Soc.*, 2021, **143**, 18041–18051.
39 Z. Liu, T. Dong, P. Mu, H. Zhang, W. Liu and G. Cui, *Chem. Eng. J.*, 2022, **446**, 136798.
40 K. Guo, S. Qi, H. Wang, J. Huang, M. Wu, Y. Yang, X. Li, Y. Ren and J. Ma, *Small Sci.*, 2022, **2**, 2100107.
41 M. D. Halls and K. Tasaki, *J. Power Sources*, 2010, **195**, 1472–1478.
42 E. G. Leggesse and J.-C. Jiang, *J. Phys. Chem. A*, 2012, **116**, 11025–11033.
43 Y.-K. Han, Y. Moon, K. Lee and Y. S. Huh, *Curr. Appl. Phys.*, 2014, **14**, 897–900.
44 Y. Yang, Y. Wang, Z. Xue, L. Zhang, L. Yan, Y. Luo and J. Xie, *J. Materiomics*, 2021, **7**, 585–592.
45 Y. Wang, Y. Lv, Y. Su, L. Chen, H. Li and F. Wu, *Nano Energy*, 2021, **90**, 106589.
46 J. Xu, Y. Li, Z. Yu, T. Le, C. Zhang and Y. Yang, *J. Mater. Sci.: Mater. Electron.*, 2020, **31**, 12249–12256.
47 S. Dai, F. Zeng, J. Zhang, X. Li and Z. Shao, *Ionics*, 2021, **27**, 4233–4240.
48 M. T. Nguyen, P. Sutton, A. Palumbo, M. G. Fischer, X. Hua, I. Gunkel and U. Steiner, *Mater. Adv.*, 2022, **3**, 362–372.
49 Q. Zhang, J. Pan, P. Lu, Z. Liu, M. W. Verbrugge, B. W. Sheldon, Y.-T. Cheng, Y. Qi and X. Xiao, *Nano Lett.*, 2016, **16**, 2011–2016.
50 X. Zheng, X. Wang, X. Cai, L. Xing, M. Xu, Y. Liao, X. Li and W. Li, *ACS Appl. Mater. Interfaces*, 2016, (8), 30116–30125.